EPJ Web of Conferences **40**, 03001 (2013)
DOI: 10.1051/epjconf/20134003001

d^0 Ferromagnetism in Oxide Nanowires: Role of Intrinsic Defects

Shyamsundar Ghosh,[1] Gobinda Gopal Khan[1] and Kalyan Mandal[1]

[1]Department of Condensed Matter Physics and Material Sciences, S. N. Bose National Centre for Basic Sciences, Block JD, Sector III, Salt Lake City, Kolkata 700 098, India.

Abstract. In this report, we have investigated the origin of defect-induced room-temperature d^0 ferromagnetism in pure SnO_2 and ZnO nanowires (NWs) with average diameter ~ 50 nm, prepared by template assisted route. Photoluminescence (PL) and electron paramagnetic resonance (EPR) spectroscopic measurements show the singly ionized oxygen vacancy is inducing ferromagnetism in pure SnO_2 NWs whereas cation (Zn) vacancy is found to responsible for the ferromagnetic behaviour in pure ZnO NWs. Besides, it is found that the Zn vacancy-induced ferromagnetism in ZnO can be tuned by substituting few percentage of non-magnetic alkali metal like potassium (K) at Zn site. Saturation moment as well as Curie temperature has found to increase significantly with K-doping up to 4 at.% but a decrease of ferromagnetic response is observed for higher K-doping. X-ray photoelectron spectra show that K^{+1} ions substitute at Zn site and thus introduce hole through which a ferromagnetic interaction between Zn vacancies can be mediated. The direct correlation between the Zn vacancy concentration and the corresponding saturation moment indicates that Zn vacancy-induced ferromagnetism in ZnO can be successfully tuned by K-doping that can an exciting approach to prepare ZnO-based dilute magnetic semiconductors for modern spintronic technology.

1 Introduction

The integration of ferromagnetism (FM) in the wide band gap oxide semiconductors has drawn intense research focus in spintronics [1]. Recently, room temperature ferromagnetism (RTFM) has been reported in the nanostructures of wide band gap pristine and different non-magnetic element doped oxide semiconductors like ZnO, HfO_2, CeO_2, SnO_2, In_2O_3 Al_2O_3 and TiO_2 [2-8]. However the origin of such unexpected FM in different oxides is found to be controversial issue [2-8]. RTFM in the nanostructures and thin films of undoped and non magnetic ion doped oxide semiconductors is attributed to different intrinsic structural defects like oxygen vacancies [2, 5, 6], cation vacancies [8] or even the surface defects [9], where the quantum confined dimensions of the nanostructures should have very important influence [2]. Therefore, the study of the origin RTFM and the tuning of the ferromagnetic properties in the pristine and non magnetic ion doped metal oxide semiconductors are very exciting considering their potential application for modern spintrionic and opto-spintronic devices.

In this work, we have studied the origin of the defect-driven RTFM in pure SnO_2 and ZnO NWs fabricated by template assisted wet chemical route. We also have prepared non magnetic alkali-ion K doped ZnO NWs in order to control the FM in the ZnO NWs. It is found that the singly ionized oxygen vacancy clusters are responsible for the FM in pure SnO_2 NWs. On the other hand, the magnetic interaction between the cation vacancies mediated via holes is attributed to the observed FM in pure and K-doped ZnO NWs.

2 Experimental details

Arrays of SnO_2 and K-doped ZnO NWs are fabricated within nanoporous anodic aluminium oxide (AAO) template through wet chemical route. A precursor solution of 0.2 M $SnCl_4.5H_2O$ and urea dissolved in ethanol is used for the preparation of SnO_2 NWs, whereas the undoped and K-doped ZnO NWs are synthesized by dipping the AAO templates in the alcoholic solutions of zinc acetate and potassium acetate. The K-doping concentration was varied by carefully by changing the atomic ratio of Zn/K in acetate solution. AAO templates were immersed in these respective mixed solution and left for few days. Then the AAO templates were removed from the precursor solution and annealed in air at 450^o C for 2 hrs. The NWs grown inside the pores of AAO template are characterized by X-ray diffraction (XRD), X-ray photoelectron spectroscopy (XPS), vibrating sample magnetometer (VSM), photoluminescence (PL) and electron paramagnetic resonance (EPR) spectroscopy. The morphology of the NWs is observed by field emission scanning electron microscope (FESEM)

after dissolving the template partially in NaOH solution to release the NWs.

3 Results and discussion

Figure 1(a) and 1(c) show the FESEM images for pure SnO_2 and 4 at.% K-doped ZnO NWs respectively which exhibit the nanowire-like morphology. High resolution FESEM images also show that both the SnO_2 and ZnO NWs have the diameter in the range of 40-50 nm which is very close to the pore diameter of AAO template. The XRD pattern of the as grown pristine SnO_2 NWs, shown in Fig. 1(d), indicates pure polycrystalline rutile SnO_2 structure (JCPDS card no. 41-1445). On the other hand, undoped and K-doped ZnO NWs show hexagonal wurtzite ZnO crystal structure, where the lattice parameters are found to increase almost linearly with K concentration due to the gradual substitution of larger K^{1+} ions (151 pm) replacing smaller Zn^{2+} ions (74 pm) inside ZnO lattice. This observation indicates the successful doping of K ions inside ZnO. Two diffraction peaks at 2θ values of 38.48 and 44.84 appear from the electropolished Al substrate underneath AAO template.

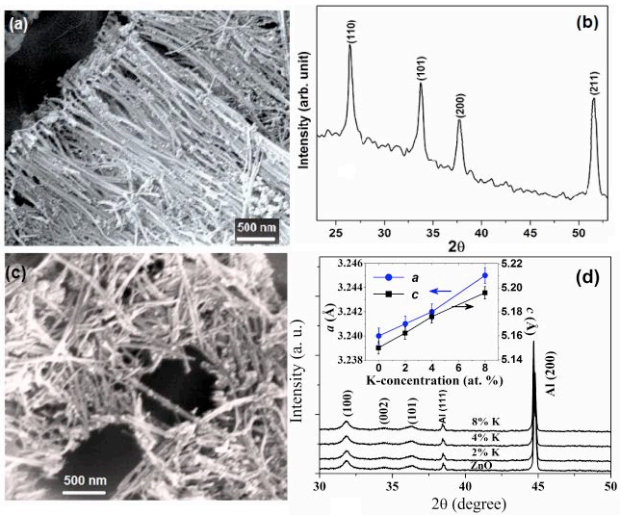

Fig.1. FESEM images of (a) pure SnO_2 and (c) 4 at.% K-doped ZnO NWs. The XRD pattern of (b) pure SnO_2 NWs and (d) 4 at.% K-doped ZnO NWs, where inset shows the variation of lattice parameters of hexagonal ZnO unit cell with K-doping concentration.

3.1 Origin of ferromagnetism in SnO_2 NWs

Pure SnO_2 NWs are found to exhibit RTFM with low saturation moment (~ 10^{-2} emu/g) as shown in Fig. 2(a) and (b) for 300 and 80 K respectively. The observed reduction of the saturation moment at higher field is due to dominance of the diamagnetic contribution from the AAO template. Similar RTFM in different oxides like ZnO, HfO_2, SnO_2, TiO_2 nanostructures is also observed in which structural defects like oxygen vacancies [2-6], cation vacancies [8], grain boundaries or interfacial defects [2, 9] are attributed to the origin of FM. Therefore to investigate the possible defects formation within the SnO_2 NWs here, PL spectroscopic measurements are performed using the excitation wavelength of 330 nm of Xe lamp. Figure 2(c) show the normalised PL spectra on the template embedded SnO_2 NWs. The AAO template itself provides a broad blue emission centred at 2.90 eV because of the oxygen vacancy related defects [10]. The SnO_2 NWs is found to exhibit an emission peak in green-yellow region centred at 2.53 eV. The origin of deep green-yellow emission in SnO_2 nanostructures can be originated from different crystalline defects such as oxygen vacancy (V_O) and Sn vacancy (V_{Sn}) [11]. Due to high formation energy of V_{Sn}, it is quite unfavourable to stabilize considerable amount of V_{Sn} defects in the pure SnO_2 without any controlled defect engineering [12]. On the other hand, V_O defects can easily grow in SnO_2 nanostructures due its low formation energy and often found to exhibit green-yellow luminescence [2, 13].

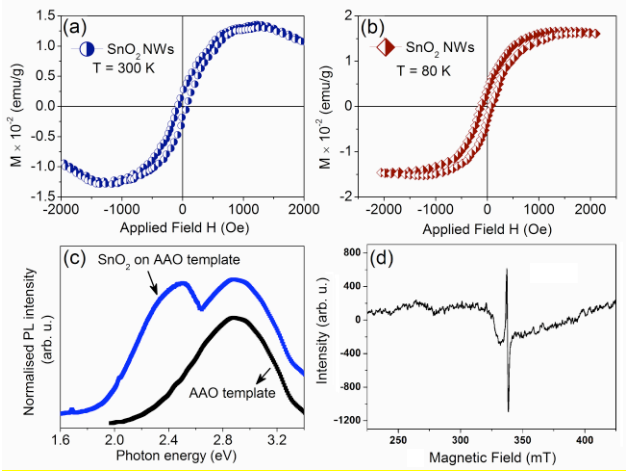

Fig.2. Magnetic hysteresis loops of pure SnO_2 NWs at (a) 300 K and (b) 80 K. Room-temperature (c) PL and (d) EPR spectra of pure SnO_2 NWs.

However, three kinds of V_O defects such as neutral oxygen vacancies (V_O^0), singly ionized oxygen vacancies (V_O^+) and doubly ionized oxygen vacancies (V_O^{++}) can form within SnO_2 nanostructures. To investigate the types of V_O defects, EPR spectroscopic measurement for pure SnO_2 NWs is conducted and the spectrum is shown in Fig. 2(d). The value of g factor is estimated using the formula $g = h\gamma/\mu_B H$, where H is the magnetic field (gauss), μ_B is the Bohr magnetron equal to 9.274×10^{-21} erg/Gauss, h is Planck's constant, 6.626×10^{-27} erg-s/cycle and γ is the frequency (Hz). The estimated value of g-factor for pure SnO_2 NWs is found to be 1.998 which is very close to 2. Recently, Özcan *et al* [14], have shown that the Sn^{+4}, Sn^{+2}, V_O^0 and V_O^{++} defect states have an even number of electrons and these are EPR-silent singlets. Based on the DFT calculations they also have demonstrated that the g factor around 2.00 can appear because of the V_O^+ defects in the SnO_2 and this defect is only EPR active [14]. Popescu *et al* [15] have also attributed the EPR signal with the g factor around 2.00 to V_O^+ defects in undoped SnO_2 nanostructures. Therefore, our EPR spectroscopy result for the pristine SnO_2 NWs suggests that the signal is originated from the V_O^+ defects, which are believed to be the recombination centres for the luminescence processes.

V_O^+ is found to have magnetic moment [2, 5] and can be the possible origin of FM in pure SnO_2 NWs. The groups of Coey *et al* [16] have shown that V_O^+ centres

(F^+ centres) or V_O^+ centre clusters form a triplet state and can initiate defect related hybridization causing charge transfer from a donor-derived impurity state to the unoccupied states at the Fermi energy level to establish a long-range ferromagnetic interaction between the V_O^+ defects. Although, the contribution from cation vacancy (V_{Sn}) defects can not be discarded completely that can also induce FM in such oxides. In our work, due to high formation energy, it is expected that the concentration of V_{Sn} should be much below the required percolation threshold to mediate long-range ferromagnetic ordering in pristine SnO_2 NWs [17]. We also have not traced any presence of V_{Sn} defects, hence we believe that the V_O^+ defect clusters are responsible for the FM ordering in pure SnO_2 NWs.

3.2 Origin of Ferromagnetism in pure and K-doped ZnO NWs

Magnetic hysteresis loops of undoped and K-doped ZnO NWs are shown in Fig. 3(a). Like pure SnO_2 NWs, here also, pure ZnO NWs also found to exhibit RTFM with magnetization higher by almost one order in magnitude compared to pure SnO_2 NWs. Interestingly, saturation magnetization (M_S) in ZnO NWs is found to enhance with the increase of K-doping concentration up to 4 at.% but then decreases for higher K-concentration. The inset of Fig. 3(a) show the temperature dependent magnetization M(T) curves for undoped ZnO and 4 at.% K-doped ZnO NWs. The estimated values of Curie temperatures (T_C) of ZnO NWs are also found to enhance with K-doping and 4 at.% K-doped ZnO NWs showed the highest $T_C \sim 510$ K like M_S.

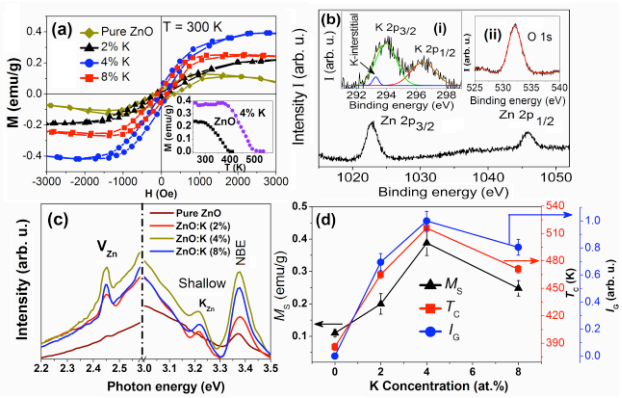

Fig.3. Room temperature magnetic hysteresis loops of pure and K-doped ZnO NWs, the inset show the high temperature magnetization M (T) curves for pure and 4 at.%K-doped ZnO NWs. (b) XPS spectra of Zn 2p , K 2p (in inset (i)) and O 1s (in inset (ii)) core levels of 4 at.% K-doped ZnO NWs. (c) RTPL spectra of doped ZnO NWs. (d) Variation of M_S, T_C and green luminescence intensity (I_G) with K-doping concentration.

The substitution of K at Zn site has been confirmed by XPS measurements. Figure 3(b) show the XPS spectrum of Zn 2p core level which display a doublet located at 1022.4 and 1045.95 eV respectively that corresponds to the core lines of Zn $2p_{3/2}$ and $2p_{1/2}$ states. The binding energy difference (23.15 eV) between the two peaks is in good agreement with the standard reference value of ZnO [18]. The estimated values of the binding energies and the binding energy difference of the Zn 2p spectrum confirm the +2 oxidation state of Zn ions [19]. The core level K 2p spectrum shown in inset (i) of Fig. 3 (b), exhibits two major peaks at 293.9 eV and 296.3 eV for K $2p_{3/2}$ and $2p_{1/2}$ states respectively that can be assigned to substitutional K (K_{Zn}) defects, whereas the low energy minor peak at 293.3 eV is due to K interstitial (K_i) defects [20]. Therefore, XPS study confirms that the majority of K ions are substituted at Zn site while a little amount of K ions are also occupying at the lattice interstitials site. The core level O 1s state, presented in the inset (ii) of Fig. 3(b), shows a peak at 532.1 eV which is originated due to Zn-O bond in the wurtzite crystal structure of the hexagonal ZnO [21].

Figure 3(c) show the normalised PL spectra of pure and K-doped ZnO NWs embedded on the AAO template. PL spectra of the template embedded pure and doped ZnO NWs are found to exhibit a broad blue emission centred at 2.90 eV originating due to AAO template [10]. Hence we have neglected the hump like broad blue region for all the K-doped ZnO NWs. It is important to notice that all the doped ZnO NWs show significant green emission (2.42 eV) along with ultraviolet-visible (UV) emission. The emission peak at 3.37 eV corresponds to the near band edge (NBE) electronic transition and/or the free exciton recombination through an exciton–exciton collision process [22]. It is noticeable that K-doping results in the enhancement of intensity of the NBE UV emission which is found to be maximum for 4 at.% K-doped ZnO NWs.

An extra emission peak is found to appear at 3.21 eV with the introduction of K in ZnO. The emission peak near to the ZnO band edge is quite expectable because of the electronic transition from conduction band minimum (CBM) to the shallow K_{Zn} acceptor levels [23-24]. The presence of the shallow K_{Zn} acceptor states can push the ZnO system from n-type to p-type direction [23]. Looking at the intensity of the peak it is clear that maximum amount of K ions are substituted at Zn site in case of 4 at.% K-doped NWs. For higher K-doping, the substitution process might get saturated and K ions can move to lattice interstitial (K_i) position which acts as a donor [23-24] and thereby can reduce the p-type nature of ZnO. Therefore, the hole concentration should maximum in the 4 at.% K-doped ZnO NWs compared to the others.

Besides the NBE emission, the K-doped NWs also exhibited significant green emission centred at 2.43 eV. The origin of well known green emission in ZnO nanostructures and thin films is highly controversial. It was previously believed that the oxygen vacancies (V_O) [25] are responsible for the green emission, but recent in depth studies reveal that Zn vacancy (V_{Zn}) is found the origin of the green emission in ZnO nanostructures and thin films [26, 27]. The green emission is attributed to the electronic transition between the CBM and V_{Zn} acceptor levels which is found to situated at 0.9 eV above the valance band maxima (VBM) [26, 27]. Therefore, K-doping is found to stabilize more V_{Zn} defects in ZnO NWs and the 4 at.% K-doped NWs contains maximum amount of V_{Zn} defects as the intensity of the green emission is highest. Similar enhancement in V_{Zn}

concentration with Li-doping in ZnO thin films is also observed previously [8].

V_{Zn} is found to have localised magnetic moment originating from the unpaired 2p orbital of O atom nearest the V_{Zn} site [3, 8] and the results so far clearly suggests that they are surely playing a crucial role in inducing FM in K-doped ZnO NWs. In fact, a direct correlation of the M_S and T_C with the green emission intensity (I_G) has observed in Fig. 3(d). It is quite interesting to notice that the increase of I_G follows the increase of M_S as well as the T_C of the K-doped ZnO NWs. The magnetic moments of V_{Zn} defects can be mediated through the holes due to K_{Zn} defects and giving rise to a long range ferromagnetic interaction. The 4 at.% K-doped NWs contains maximum amount of V_{Zn} and holes and this is the reason it show the strongest FM. With the increase of K-doping concentration, the advent of K-interstitial defects compensates the acceptor-like defects such as K_{Zn} and V_{Zn} and thereby reducing the overall hole concentration and consequently the strength of FM.

4 Conclusions

In summary, the origin of FM in pure SnO_2 and K-doped ZnO NWs has been successfully investigated. Singly ionized oxygen vacancies are found to induce RTFM in pure SnO_2 NWs. On the other hand, cation vacancies (V_{Zn}) is playing a role in stabilizing FM in ZnO NWs and the FM signature is found to enhance with the substitution of alkali-element K at Zn site. The concentrations Zn vacancies as well as the p-type conductivity of the ZnO NWs are found to increase significantly with K-doping and the FM signature increases consequently. For higher K-doping concentration, the stabilization donor like K-interstitial defects compensates the effects of K-substitutional and Zn vacancy acceptors and thereby reducing the degree of p-type nature which diminishes the related FM consequently. Therefore, the stabilization of defect-induced FM in such oxides can be an exciting approach to prepare new class of magnetic semiconductors for spintronics and opto-spintronics applications.

Acknowledgements

One of the authors (S. G.) thanks Council of Scientific and Industrial Research (CSIR), Government of India, for providing a research fellowship. The above work is supported by the CSIR (INDIA) funded project 03(1178)/10/EMR-II.

References

1. H. Ohno, Science 281, 951 (1998)
2. A. Sundaresan, R. Bhargavi, N. Rangarajan, U. Siddesh and C. N. R. Rao, Phys. Rev. B 74, 161306(R) (2006)
3. Q. Wang, Q. Sun, G. Chen, Y. Kawazoe and P. Jena, Phys Rev. B 77, 205411 (2008)
4. M.Venkatesan, C. B. Fitzgerald and J. M. D. Coey, Nature 430, 630 (2004)
5. R. Podila, W. Queen, A. Nath, J. T. Arantes, A. L. Schoenhalz, A. Fazzio, G. M. Dalpian, J. He, S. J. Hwu, M. J. Skove and A. M. Rao, Nano Lett. 10, 1383 (2010)
6. S. Ghosh, D. De. Munshi and K. Mandal, J. Appl. Phys. 107, 123919 (2010)
7. S. Ghosh, Gobinda Gopal Khan, and K. Mandal, ACS Appl. Mater. Interfaces 4, 2048 (2012)
8. J. B. Yi, C. C. Lim, G. Z. Xing, H. M. Fan, L. H. Van, S. L. Huang, K. S. Yang, X. L. Huang, X. B. Qin, B.Y. Wang, T. Wu, L. Wang, H. T. Zhang, X.Y. Gao, T. Liu, A. T. S. Wee, Y. P. Feng and J. Ding, Phys. Rev. Lett. 104, 137201 (2010)
9. J. B. Yi, H. Pan, J. Y. Lin, J. Ding, Y. P. Feng, S. Thongmee, T. Liu, H. Gong, and L. Wang, Adv. Mater. 20, 1170 (2008)
10. G.G. Khan, N. Mukherjee, A. Mondal, N.R. Bandyopadhyay, A. Basumallick, Mats. Chem. Phys. 122, 60 (2010)
11. H. He, T.H. Wu, C.L. Hsin, K.M. Li, L.J. Chen, Y.L. Chueh, L.J. Chou, Z.L. Wang, Small 2, 116 (2006)
12. C. Kilic, A. Zunger, Phys. Rev. Lett. 88, 095501(2002)
13. S. Luo, P.K. Chu, W. Liu, M. Zhang, C. Lin, Appl. Phys. Lett. 88, 183112 (2006)
14. N. Özcan, T. Kortelainen, V. Golovanov, T.T. Rantala, J. Vaara, Phys. Rev. B 81 235202 (2010)
15. D.A. Popescu, J.M. Herrmann, A. Ensuque, F. Bozon-Verduraz, Phys. Chem. Chem. Phys. 3, 2522 (2001)
16. J.M.D. Coey, M. Venkatesan, C. B. Fitzgerald, Nature Mats. 4, 173 (2005)
17. X. Liu, J. Iqbal, Z. Wu, B. He, R. Yu, J. Phys. Chem. C 4790, 114 (2010)
18. C. D. Wagner, W. M. Riggs, L.E. Davis, J. F. Moulder, G. E. Muilenberg, in: Handbook of X-ray Photoelectron Spectroscopy, Perkin Elmer, Eden Prairie, 1979.
19. D. K. Mishra, P. Kumar , M. K. Sharma , J. Das , S. K. Singh , B. K. Roul, S. Varma, R. Chatterjee, V. V. Srinivasu, D. Kanjilal, Physica B 405, 2659 (2010)
20. Chastain J (1992) Handbook of X-ray photoelectron spectroscopy. Perkin, Eden Prairie, MN, USA
21. Z. B. Gu, M. H. Lu, J. Wang, D. Wu, S. T. Zhang, X. K. Meng, Y. Y. Zhu, S. N. Zhu, and Y. F. Chena, Appl. Phys. Lett. 88, 082111 (2006)
22. Y.C. Kong, D.P. Yu, B. Zhang, W. Fang, S.Q. Feng, Appl. Phys. Lett. 78, 407 (2001)
23. C. H. Park, S. B. Zhang, and S. H. Wei, Phys. Rev. B 66, 073202 (2002)
24. E. C. Lee and K. J. Chang, Phys. Rev. B 70, 115210 (2004)
25. Y. Li, G.W. Meng, L.D. Zhang, Appl. Phys. Lett. 76, 2011 (2000)
26. A. Janotti and C. G. Van de Walle, Rep. Prog. Phys. 72, 126501 (2009)
27. A.F. Kohan, G. Ceder, D. Morgan and Chris G. Van de Walle, Phys. Rev. B 61, 15019 (2000)